Burn severity and vegetation type control phosphorus concentration, molecular composition, and mobilization

Morgan E. Barnes[1], J. Alan Roebuck, Jr[2], Samantha Grieger[2], Paul J. Aronstein[3], Vanessa A. Garayburu-Caruso[1], Kathleen Munson[2], Robert P. Young[1], Kevin D. Bladon[4], John D. Bailey[4], Emily B. Graham[1,5], Lupita Renteria[1], Peggy A. O'Day[3], Timothy D. Scheibe[1], Allison N. Myers-Pigg[2,6]

1 Pacific Northwest National Laboratory, Richland, WA, USA
2 Pacific Northwest National Laboratory, Sequim, WA, USA
3 Environmental Systems, University of California - Merced, Merced, CA, USA
4 College of Forestry, Oregon State University, Corvallis, OR, USA
5 School of Biological Sciences, Washington State University, Pullman, WA, USA
6 Department of Environmental Sciences, University of Toledo, Toledo, OH, USA

Correspondence to:
Allison Myers-Pigg (allison.myers-pigg@pnnl.gov)
Morgan Barnes (morgan.barnes@pnnl.gov)

Present Addresses:
J. Alan Roebuck, Jr – U.S. Geological Survey, Lower-Mississippi-Gulf Water Science Center, Nashville, TN, 37211
Robert P. Young – Washington River Protection Solutions, P.O. Box 850 MSIN M0-01, Richland, WA 99354

Supplemental Information

Carbon and Nitrogen Concentration Methods

Total carbon (C) and nitrogen (N) of the solid samples were measured on an elemental analyzer (ECS 8020; NC technologies, Italy). Leachate aqueous phase dissolved organic carbon (DOC) and total dissolved nitrogen (TDN) were determined on a Shimadzu TOC-L Total Organic Carbon Analyzer.

NMR Methodology

Solution ^{31}P nuclear magnetic resonance (NMR) experiments were run at the Environmental Molecular Science Laboratory (Pacific Northwest National Laboratory Richland Campus) on an Agilent DD2 spectrometer operated at a field strength of 14.1 T (600.18 MHz ^1H, 242.95 MHz ^{31}P) using a Varian 5 mm direct detect probe. A standard one-dimensional (1D) pulse and acquire experiment was employed using a 90° hard pulse (calibrated using the orthophosphate naturally present in each sample), an acquisition time of 0.6 s (6,098 complex points), a spectral width of 42 ppm (10.2 kHz), and relaxation delay equal to 5 times the measured T_1 relaxation constant minus the acquisition time. Each experiment was acquired for approximately 16 hours and the number of transients co-added for each spectrum was dependent on the T_1 for each individual sample.

Post-acquisition processing included setting the orthophosphate peak to 6.0 ppm, phasing, baseline correction, and line-broadening of 10 Hz using MNova 14.0.1 (Mestrelab Research, Spain). Chemical shifts of P species were compared to published literature for identification and assignments were confirmed via spiking experiments.(Cade-Menun, 2015; Doolette et al., 2009) Spiking experiments were conducted by sequentially adding solutions containing known compounds from commercial sources (Figure S2). These known P compounds were dissolved in the reconstitution buffer at concentrations of approximately 60 mM and added in 5–10 µL amounts to samples after initial sample NMR measurements. Spiked compounds, along with their chemical shifts and standard deviations, included DL-α-glycerophosphate (4.92 ± 0.05 ppm), β-glycerophosphate (4.58 ± 0.03 ppm), RNA (4.50 ± 0.06 ppm, 4.33 ± 0.03 ppm; mononucleotide degradation products), glucose-6-phosphate (5.15 ± 0.01 ppm), glucose-1-phosphate (3.27 ppm), phytate (5.58 ± 0.02 ppm, 4.60 ± 0.02 ppm, 4.30 ± 0.20 ppm, 3.89 ± 0.02 ppm), phosphocholine (3.90 ± 0.01 ppm), and adenosine monophosphate (4.42 ± 0.05 ppm).

Organic P moieties were grouped into orthophosphate monoester (monoester) or orthophosphate diester (diester) regions (Figure S2). The monoester region relative percent was calculated by integrating from 10.0 to 2.5 ppm and subtracting the orthophosphate (6 ppm) peak area. The diester region was integrated from 2.5 to -2.2. Degradation of diesters (RNA and phospholipids) to monoesters occurs in the highly alkaline extraction and reconstitution solutions and may continue during the duration of the NMR experiment.(Doolette et al., 2009; Turner et al., 2003) As a result, we corrected for this by shifting the deconvoluted areas of α-glycerophosphate, β-glycerophosphate, and mononucleotide peaks from the monoester to diester region.(Cade-Menun, 2015; Recena et al., 2018) Specific P moieties were identified and quantified with the peak picking function and any missing peaks were added by hand.

XANES Methodology

Finely ground unburned solid and char samples and reference compounds were smeared to form a homogeneous thin film on P-free tape and then mounted to an aluminum sample holder. Bulk spectra were collected in a helium gas environment at room temperature until adequate signal to noise ratio was achieved (between 2 to 16 scans). A monochromator consisting of double crystal Si (III) and spectra were recorded in fluorescence mode using a 7 element Vortex detector.

Multiple internal reference compounds were used; spectra were energy shifted for the white line of hydroxyapatite to occur at 2152.3 eV, sodium phosphate monobasic at 2152.7, and sodium pyrophosphate at 2152.5. Spectral scans were averaged in SixPack(Webb, 2005), followed by energy calibration and normalization using the Athena Software Program.(Ravel and Newville, 2005) Phosphorus speciation was estimated first with the fit_athena function in the R package 'LCF'(Werner F, 2017) using all reference compounds ($n = 46$) and samples ($n = 64$) in Grieger et al.(Grieger et al., 2022) to identify a subset of likely compounds solid samples are composed of ($n = 26$; Table S3). This subset of reference compounds was used to perform linear combination fits in Athena (Figure S3).

Previous studies have noted that differentiating reference compound spectra in complex matrices can be challenging, particularly among organic P species.(Kruse et al., 2015) However, lack of inclusion of multiple organic and inorganic compounds of a given metal within the reference compound library can result in erroneous fits and underestimation of the contributions from metal and organic P species.(Prietzel and Klysubun, 2018) Hence, we collected a large reference library of inorganic and organic species associated with Ca, Al, Fe, Mn, K, and Na and then

classified individual reference compounds into groups based on the associated metal for inorganic P (P_i) and kept all organic P (P_o) as a separate category regardless of the metal association in the linear combination fit (Figure S3; Table S3).

Method Limitations

NMR and XANES are complimentary techniques that help to gain a better understanding of Po and Pi species in environmental samples. NMR allows for measuring the detailed composition of the organic pool, such as differentiating DNA from phytate, but is only capable of classifying inorganic species as orthophosphate and polyphosphates (such as pyrophosphate). NMR has better resolution for P_o when conducted in solution, which requires extracting solid samples and potentially altering them or leaving some P unextracted.(Cade-Menun, 2015) On the other hand, XANES has the advantage of measuring the bonding environment of all P atoms in unaltered solid samples, however there are challenges to identifying organic P species(Kruse et al., 2015) (see discussion in SI XANES Methodology section). Although we used both of these techniques on the solid samples, the NMR extraction efficiencies indicate we are quantifying as low as 41.5 (16.2)% for Douglas fir forest high severity chars (Table S1). Notably, the extraction efficiencies significantly decreased as Ca-Pi (measured by XANES) increased (linear model: $p < 0.001$, $r^2 =$ 0.46), which is poorly soluble in alkaline solutions and has been observed in soil studies.(McDowell et al., 2007) Therefore, we are preferentially extracting Po and other non-Ca-containing compounds, which are primarily found in unburned and lower severity char samples. This means we are underestimating Pi in char samples when quantified by NMR relative to XANES.

Figure S1. Representative photos of Douglas-fir forest (composed of litter and live plant material) and Sagebrush shrubland (composed of big sagebrush) for each burn severity classification. Sagebrush shrubland did not reach high severity in our open-air burn experiments.

Burn Severity	Vegetation	P (%)	n
Unburned	Douglas-fir forest	87.4 (7.0)	2
	Sagebrush shrubland	105.9	1
Low	Douglas-fir forest	44.9 (14.1)	5
	Sagebrush shrubland	74.5 (13.3)	2
Moderate	Douglas-fir forest	43.5 (21.6)	3
	Sagebrush shrubland	61.0 (9.8)	2
High	Douglas-fir forest	41.5 (16.2)	4

Table S1. The P extraction efficiency mean (standard deviation) is reported as the proportion (%) of total P in the NaOH-EDTA extracts from solution ^{31}P NMR analysis relative to the aqua-regia digested solid samples. The number of samples (n) is also reported.
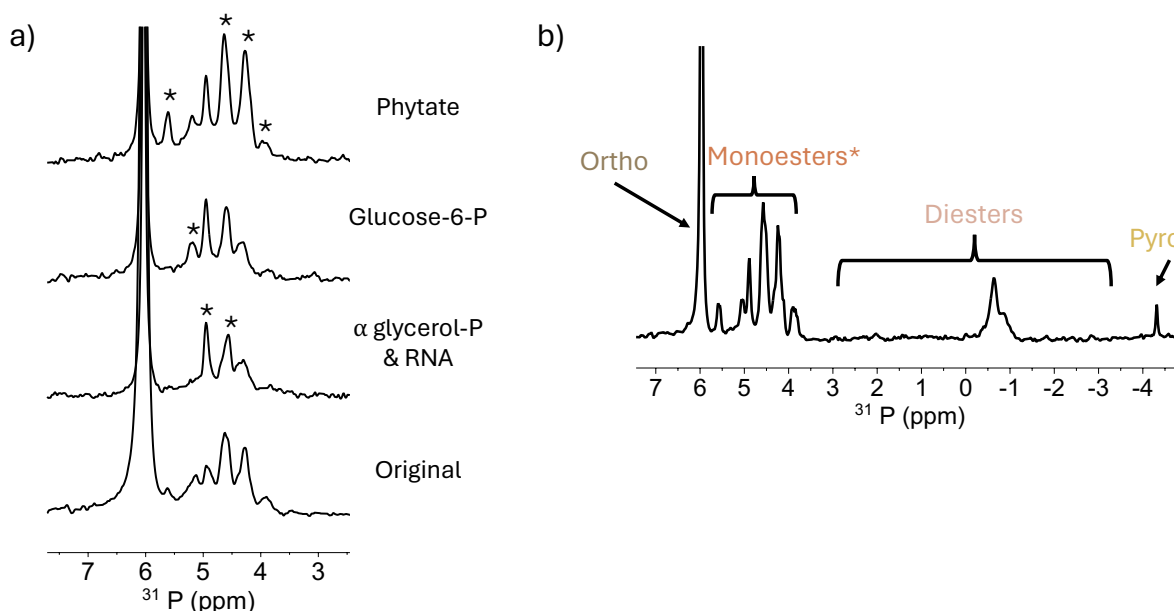
Figure S2. ^{31}P solution NMR a) an example spiking experiment showing the original sample that was subsequently spiked with DL-α-glycerophosphate (4.92 ± 0.05 ppm), RNA (4.50 ± 0.06 ppm, 4.33 ± 0.03 ppm; mononucleotide degradation products), glucose-6-phosphate (5.15 ± 0.01 ppm), and phytate (5.58 ± 0.02 ppm, 4.60 ± 0.02 ppm, 4.30 ± 0.20 ppm, 3.89 ± 0.02 ppm) to identify sample composition of the monoester region; and b) identification of orthophosphate (6 ppm), monoester region (10.0 to 2.5 ppm), diester region (2.5 to -2.2 ppm), and pyrophosphate (-4.2 ± 0.07 ppm). Orthophosphate and pyrophosphate are inorganic species (brown colors) and monoester and diesters are organic species (orange colors). Chemical shifts are reported as the mean (standard deviation) across all samples and spectra are presented with 10 Hz line broadening. *Note the monoester region may contain diester degradation products, which were corrected for. See SI NMR Methods and Method Limitation sections for additional details.
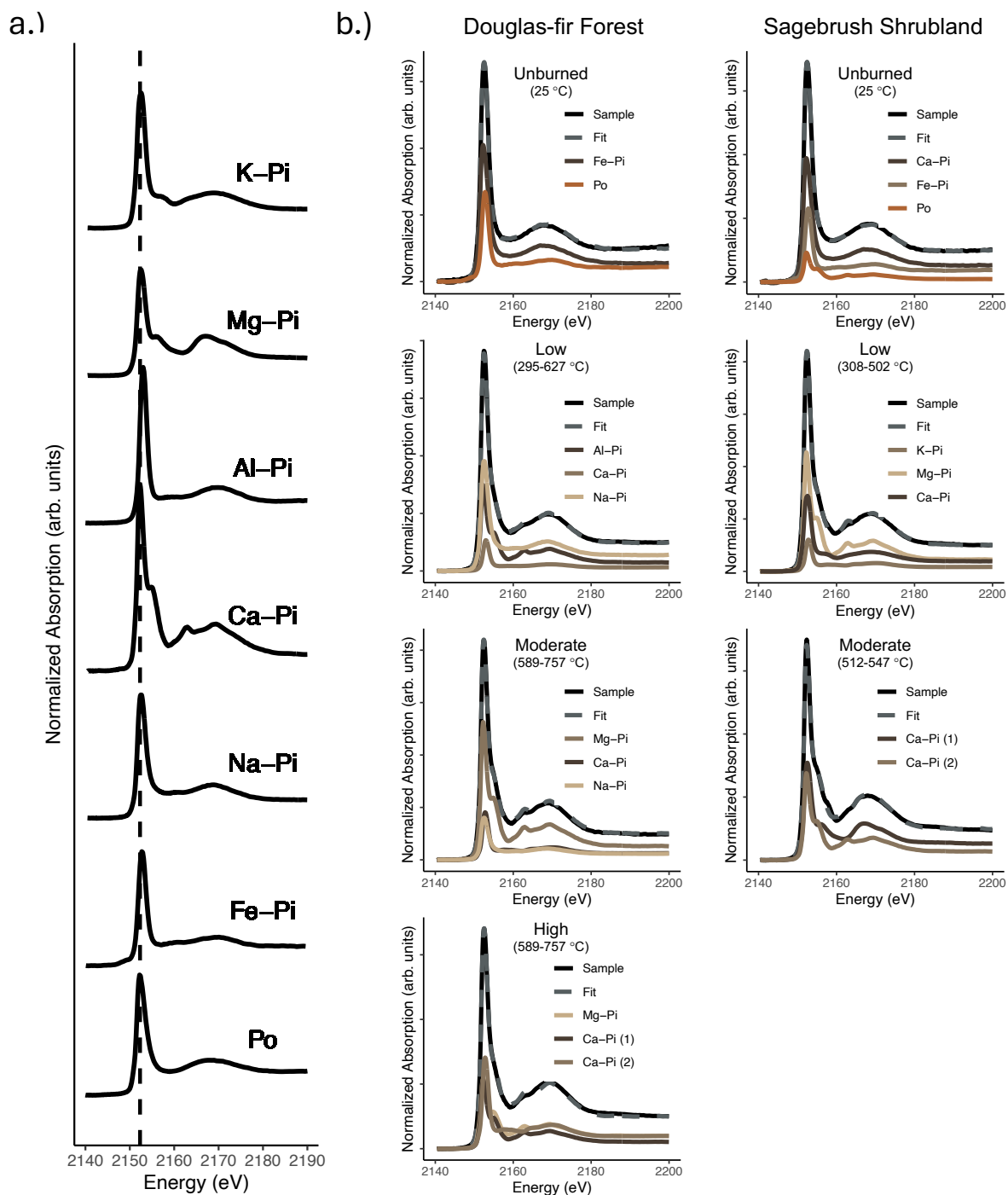
Figure S3. Phosphorus K-edge XANES (a) reference compounds representing K, Mg, Al, Ca, Na, and Fe inorganic P (Pi) along with an organic P species (Po). The vertical dashed line represents the white line of hydroxyapatite at 2152.3 eV, which was used as an internal reference compound; and (b) example linear combination fits for each burn severity experienced by Douglas-fir forest and Sagebrush shrubland. Data (black line), linear combination best fit (dashed gray line), and spectral deconvolution of the reference compounds (colored lines) are presented.

Burn Severity	Vegetation	#	Al-GibbSorb (Al-Pi)	Apatite-CaDefHydroxy (Ca-Pi)	Apatite-Carbonate (Ca-Pi)	Ca-Octa (Ca-Pi)	Ca-Tri (Ca-Pi)	Fe-FerriSorb (Fe-Pi)	Fe-GoethSorb (Fe-Pi)	K-Di (K-Pi)	K-Pyro (K-Pi)	Mg-Di (Mg-Pi)	Mg-Tri (Mg-Pi)	NH4-Mg (Mg-Pi)	Na-Tri (Na-Pi)	Ca-Lecit (Po)	Na-AMP (Po)	Sum	R Factor
Unburned	Douglas-fir forest	12	0	5.1	0	0	0	0	36.8	0	0	0	0	0	0	0	60.7	102.6	0.00058
		13	0	0	0	0	0	0	43.3	0	0	0	0	0	0	0	57.8	101.1	0.00078
	Sagebrush shrubland	14	0	9	0	0	0	0	37.1	0	0	0	0	0	0	0	55.1	101.2	0.00031
Low	Douglas-fir forest	1	0	27.9	0	0	0	0	0	0	0	0	38.2	0	0	34	0	100.1	0.00039
		7	12.7	29.7	0	0	0	0	0	0	0	0	0	0	57.1	0	0	99.5	0.00047
		8	8.7	31	0	0	0	0	0	0	0	0	0	0	62	0	0	101.7	0.00062
		10	0	39.6	0	0	0	11.8	0	0	0	0	0	0	48.7	0	0	100.1	0.00037
		51	0	40	0	0	0	0	0	0	0	0	26.1	0	32.7	0	0	98.8	0.00053
	Sagebrush shrubland	9	0	37.6	0	0	0	0	0	0	0	0	0	23	39.7	0	0	100.3	0.00103
		11	0	45.2	0	0	0	0	0	0	39.4	0	17.2	0	0	0	0	101.8	0.00064
Moderate	Douglas-fir forest	2	0	52.3	0	0	0	0	0	0	0	0	25.7	0	24	0	0	102	0.00069
		52	0	39.3	0	0	0	0	0	0	0	0	40.5	0	0	20.6	0	100.4	0.00052
		58	8.9	44.8	0	0	0	0	0	0	0	0	0	0	44.1	0	0	97.8	0.00048
	Sagebrush shrubland	68	0	27.4	0	17.7	0	0	0	0	0	0	0	0	53.6	0	0	98.7	0.00119
		72	0	27.3	17.7	0	0	0	0	0	0	0	0	0	53.7	0	0	98.7	0.00225
High	Douglas-fir forest	50	0	21.1	0	0	39.6	0	0	0	0	0	40	0	0	0	0	100.7	0.00092
		67	0	53.6	0	0	0	0	0	28	0	17.6	0	0	0	0	0	99.2	0.00074
		71	0	55.6	0	0	0	0	0	0	0	0	33.8	0	0	10.2	0	99.6	0.00058
		73	0	41.1	0	0	0	0	34.8	0	0	0	24.4	0	0	0	0	100.3	0.00072

Table S2. XANES linear combination fit results for solid samples. Samples are grouped by their burn severity, vegetation type, and sample number (as used in data packages.(Grieger et al., 2022) Only reference compounds identified in the samples are reported. See Table S3 for reference compound details, including the molecular composition. The groupings (i.e., Al-Pi, Ca-Pi, Fe-Pi, K-Pi, Mg-Pi, Na-Pi, and Po) are reported next to the reference compound name. The relative percentage (%), sum of all components, and R Factor (goodness of fit measurement) are reported for each sample individually.

Classification	File Name	Compound Name	Supplier (if Purchased) or Synthesized	CAS	Molecular Formula	Beamline	Mode	Reference
Pi_Al	Pi_Al_GibbSorb_std.xmu	Phosphate Sorbed on Gibbsite	Synthesized	N/A	N/A	SSRL 14-3	Fluorescence	O'Day et al. 2020
Pi_Ca	Pi_Apatite_CaDefHydroxy_std.xmu	Calcium-Deficient Apatite (Low Temp)	Clarkson	N/A	Varies	SSRL 14-3	Fluorescence	This Study
	Pi_Apatite_Carbonate_std.xmu	Carbonate Apatite	Clarkson	N/A	$(Ca_{10-x}Ha_x)(PO_4)_{6-x}(CO_3)_x(OH)_2$	CLS SXRMB	Fluorescence	Barnes, 2020
	Pi_Ca_Mono_std.xmu	Calcium Phosphate Monobasic Monohydrate	Sigma Aldrich	10031-30-8	$Ca(H_2PO_4)2 \cdot H2O$	SSRL 14-3	Fluorescence	This Study
	Pi_Ca_Octa_std.xmu	Octacalcium Phosphate	Clarkson	13767-12-9	$Ca_8H_2(PO_4)_6 \cdot 5H_2O$	CLS SXRMB	Fluorescence	Barnes, 2020
	Pi_Ca_Pyro_std.xmu	Amorphous Calcium Pyrophosphate	Aldrich	7790-76-3	$Ca_2O_7P_2 \cdot H_2O$	SSRL 14-3	Fluorescence	This Study
	Pi_Ca_Tri_std.xmu	Calcium Phosphate Tribasic	Acros Organics	7758-87-4	$Ca_3O_8P_2$	SSRL 14-3	Fluorescence	This Study
Pi_Fe	Pi_Fe_FerriSorb_std.xmu	Phosphate Sorbed on Ferrihydrite	Synthesized	N/A	N/A	SSRL 14-3	Fluorescence	O'Day et al. 2020
	Pi_Fe_GoethSorb_std.xmu	Phosphate Sorbed on Goethite	Synthesized	N/A	N/A	CLS SXRMB	Fluorescence	O'Day et al. 2020
	Pi_Fe_Precip_std.xmu	Precipitated Iron Phosphate	Synthesized	N/A	N/A	CLS SXRMB	Fluorescence	Barnes, 2020
Pi_K	Pi_K_Di_std.xmu	Potassium Phosphate Dibasic Anhydrous	Fisher	7758-11-4	K_2HPO_4	SSRL 14-3	Fluorescence	This Study
	Pi_K_Pyro_std.xmu	Potassium Diphosphate; Potassium Pyrophosphate	Acros Organics	7320-34-5	$K_4P_2O_7$	SSRL 14-3	Fluorescence	This Study
Pi_Mg	Pi_Mg_Di_std.xmu	Magnesium Hydrogen Phosphate Trihydrate; Magnesium Phosphate Dibasic Trihydrate	Sigma Aldrich	7782-75-4	$MgHPO_4 \cdot 3H_2O$	SSRL 14-3	Fluorescence	This Study
	Pi_Mg_Tri_std.xmu	Magnesium Phosphate Tribasic Hydrate	Thermo Scientific	53408-95-0	$Mg_3(PO_4)_2 \cdot xH_2O$	SSRL 14-3	Fluorescence	This Study
	Pi_NH4_Mg_std.xmu	Ammonium Magnesium Phosphate Hydrate; Struvite	Alfa Aesar	7785-21-9	$(NH_4)MgPO_4 \bullet xH_2O$	SSRL 14-3	Fluorescence	This Study
Pi_Na	Pi_Na_Tri_std.xmu	Sodium Phosphate Tribasic Dodecahydrate	Fisher	10101-89-0	$H_{24}Na_3O_{16}P$	SSRL 14-3	Fluorescence	This Study
Pi_NH4	Pi_NH4_Mono_std.xmu	Ammonium Dihydrogen Phosphate; Ammonium Phosphate Monobasic	Acros Organics	7722-76-1	$NH_4H_2PO_4$	SSRL 14-3	Fluorescence	This Study

Po	Po_Al_DNA_GibbSorb_2_std.xmu	DNA Sorbed on Gibbsite	Synthesized	N/A	N/A	CLS SXRMB	Fluorescence	O'Day et al. 2020
	Po_Al_DNA_GibbSorb_std.xmu	DNA Sorbed on Gibbsite	Synthesized	N/A	N/A	CLS SXRMB	Fluorescence	Barnes, 2020
	Po_Ca_Lecithin_std.xmu	Lecithin (90% Soybean); Phosphatidylcholine	Alfa Aesar	8002-43-5	$C_{42}H_{80}NO_8P$	CLS SXRMB	Fluorescence	Barnes, 2020
	Po_Fe_PA_FerriSorb_std.xmu	Phytic Acid Sorbed on Ferrihydrite	Synthesized	N/A	N/A	CLS SXRMB	Fluorescence	Barnes, 2020
	Po_Fe_PA_GoethSorb_std.xmu	Phytic Acid Sorbed on Goethite	Synthesized	N/A	N/A	CLS SXRMB	Fluorescence	Barnes, 2020
	Po_Na_AMP_std.xmu	Adenosine 5'-Monophsphate Sodium Salt (Yeast)	Sigma	149022-20-8	$C_{10}H_{14}N_5O_7P \cdot xNa^+ \cdot yH_2O$	CLS SXRMB	Fluorescence	Barnes, 2020
	Po_Na_ATP_std.xmu	Adensosine-5'-Triphosphate Disodium Salt Hydrate	Alfa Aesar	34369-07-8	$C_{10}H_{14}N_5Na_2O_{13}P_3 \cdot xH2O$	CLS SXRMB	Fluorescence	Barnes, 2020
	Po_Na_DNA_std.xmu	Deoxyribonucleic Acid Sodium Salt (Salmon Testes)	Sigma	438545-06-3	N/A	CLS SXRMB	Total Electron Yield	Barnes, 2020
	Po_Na_PA_std.xmu	Phytic Acid Sodium Salt Hydrate (Rice)	Sigma Aldrich	14306-25-3	$C_6H_{18}O_{24}P_6 \cdot xNa+ \cdot yH_2O$	CLS SXRMB	Total Electron Yield	Barnes, 2020

Table S3. X-ray absorption near edge structure (XANES) reference compounds list used for linear combination fitting in Athena. Inorganic P species (Pi) were grouped based on metal association, whereas organic P (Po) species were grouped together regardless of the metal association (see XANES methodology in SI for additional details). Additional information includes file names, the full compound name, the supplier, CAS number, molecular formula, beamline data was collected on, collection mode, and citation spectra was acquired from. Additional reference compounds were used for initial linear combination fits and can be found in Grieger et al.(Grieger et al., 2022)
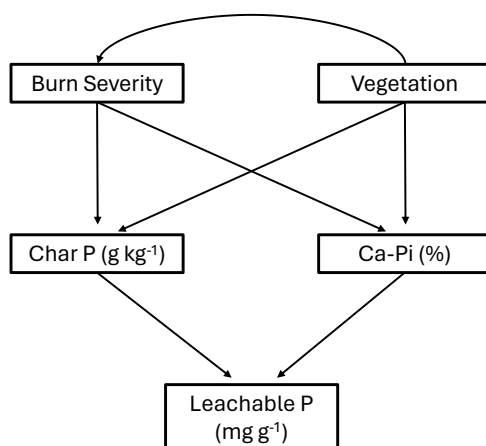
Figure S4. Path analysis conceptual model of hypothesized relationships between burn severity, vegetation type, and leachable P.

Burn Severity	Vegetation	Burn Duration (Minutes)	Lowest Max Temp (°C)	Highest Max Temp (°C)	n
Unburned	Douglas-fir forest	NA	25	25	2
	Sagebrush shrubland	NA	25	25	1
Low	Douglas-fir forest	342 (403)	295	627	5
	Sagebrush shrubland	131 (104)	308	512	2
Moderate	Douglas-fir forest	456 (303)	589	757	3
	Sagebrush shrubland	202 (3)	512	547	2
High	Douglas-fir forest	783 (195)	589	757	4

Table S4. Burn characteristics for severity classifications for each vegetation type including mean (standard deviation) duration, mean (standard deviation) maximum temperature reached, low and high range of maximum temperature, and sample count.
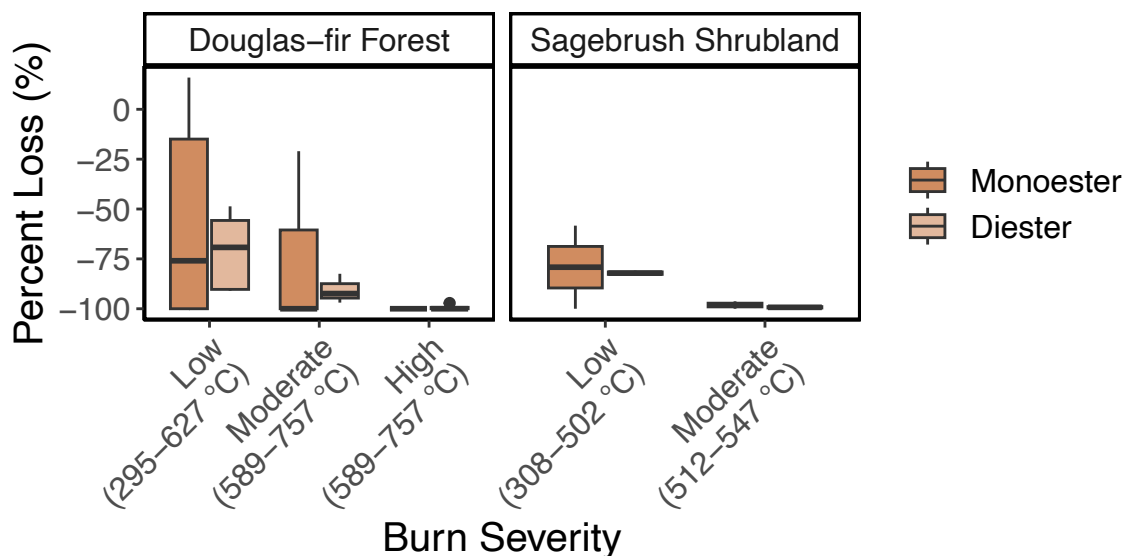
Figure S5. Percent loss of monoester (dark pink) and diester (light pink) species, as identified by ^{31}P NMR. Analysis of variance found no significant difference ($p = 0.97$) between organic classes for the three-factor interaction term. This indicates monoester and diester species are lost at similar proportions within a burn severity classification and vegetation type.

Burn Severity	Vegetation	Ortho	PL	RNA	G6P	Phytate	DNA	Pyro
		Percent (%)						
Unburned	Douglas-fir forest	56.8 (2.5)	15.9 (11.2)	9.3 (4.03)	0.7 (NA)	12.4 (NA)	11.3 (0.8)	2.7 (0.8)
	Sagebrush shrubland	44.8 (NA)	10.7 (NA)	4.9 (NA)	2.7 (NA)	23.2 (NA)	14.1 (NA)	1.5 (NA)
Low	Douglas-fir forest	73.9 (9.4)	3.2 (1.5)	7.2 (5.7)	0.6 (0.2)	3.6 (0.2)	2.4 (0.5)	13.6 (3.1)
	Sagebrush shrubland	79.7 (14.7)	1.4 (0.4)	2.2 (2.8)	4.6 (NA)	5.5 (4.1)	2.2 (0.7)	9.9 (6.2)
Moderate	Douglas-fir forest	87.2 (8.8)	1.5 (1.3)	2.6 (2.8)	0.4 (NA)	2.4 (NA)	0.8 (NA)	8.3 (4.7)
	Sagebrush shrubland	97.2 (0.8)	0.1 (0.1)	0.3 (NA)	0	0	0	2.1 (1.3)
High	Douglas-fir forest	95.9 (1.6)	0.1 (0.1)	0.9 (NA)	0	0	0	3.8 (1.5)

Table S5. Mean (standard deviation) of molecular moieties identified by ^{31}P NMR in Douglas-fir forest and sagebrush shrubland solid samples across the burn severity gradients. Molecular moieties include orthophosphate (ortho), phospholipids (PL), RNA, glucose-6-phosphate (G6P), phytate, DNA, and pyrophosphate (pyro).

Burn Severity	Vegetation	P	Ca	Fe	Al	K	Mg	Na	S	C	N	n
						g kg^{-1}						
Unburned	Douglas-fir forest	1.29 (0.52)	4.89 (1.23)	0.52 (0.30)	0.64 (0.42)	4.57 (2.20)	0.97 (0.14)	0.17 (0.03)	0.76 (0.22)	340.05 (11.53)	11.05 (2.90)	2
	Sagebrush shrubland	1.27	4.08	1.05	1.01	10.79	1.34	0.25	1.01	341.9	8.4	1
Low	Douglas-fir forest	1.83 (0.73)	14.75 (3.01)	0.93 (0.22)	0.95 (0.44)	7.59 (3.15)	1.66 (0.55)	0.30 (0.03)	0.45 (0.20)	180.18 (68.62)	4.98 (2.06)	5
	Sagebrush shrubland	4.91 (1.34)	18.60 (6.88)	3.55 (1.41)	3.37 (1.55)	40.84 (10.78)	4.50 (1.70)	0.69 (0.36)	2.37 (1.06)	200.80 (18.10)	9.35 (0.78)	2
Moderate	Douglas-fir forest	2.33 (0.71)	20.65 (5.98)	1.25 (0.87)	1.38 (0.75)	9.73 (2.66)	2.24 (0.76)	0.36 (0.14)	0.50 (0.26)	161.13 (100.15)	5.47 (1.86)	3
	Sagebrush shrubland	14.45 (3.48)	52.47 (12.09)	11.01 (0.03)	10.39 (1.20)	118.51 (28.55)	13.37 (1.87)	2.10 (0.32)	5.67 (0.88)	154.95 (29.63)	5.30 (0.99)	2
High	Douglas-fir forest	6.20 (1.94)	51.60 (16.59)	3.37 (1.29)	3.59 (1.42)	24.91 (8.00)	5.75 (1.84)	0.84 (0.31)	1.14 (0.41)	129.30 (46.06)	5.13 (2.83)	4

Table S6. Solid sample elemental concentration (P, Ca, Fe, Al, K, Mg, Na, S, C, and N; g kg^{-1}) mean (standard deviation) based on burn severity and vegetation type.

Burn Severity	Vegetation	Sample Phase	Ca:P	Mg:P	Fe:P	Al:P	Na:P	K:P	S:P	C:P	N:P
Unburned	Douglas-fir forest	Solid	3.3 (2.1)	1.1 (0.6)	0.3 (0.2)	0.7 (0.7)	0.2 (0.1)	2.7 (0.2)	0.6 (0.1)	732.2 (271.0)	19.5 (2.9)
		Particulate	1.0 (0.5)	0.6 (0.4)	0.6 (0.8)	0.9 (1.1)	0.1 (ND)	5.5 (5.8)	0.2 (0.1)	ND (ND)	ND (ND)
		Aqueous	0.5 (0.2)	0.4 (0.1)	0.0 (0.0)	0.1 (0.0)	0.7 (0.6)	7.2 (0.9)	0.2 (0.0)	83.4 (27.2)	1.5 (0.3)
	Sagebrush shrubland	Solid	2.5 (ND)	1.4 (ND)	0.5 (ND)	0.9 (ND)	0.3 (ND)	6.8 (ND)	0.8 (ND)	696.5 (ND)	14.7 (ND)
		Particulate	2.9 (2.0)	3.1 (2.5)	3.9 (3.9)	5.5 (5.8)	0.5 (0.5)	14.1 (6.9)	0.5 (ND)	ND (ND)	ND (ND)
		Aqueous	0.8 (0.0)	0.5 (0.0)	0.0 (0.0)	0.0 (0.0)	0.1 (0.0)	6.1 (0.0)	0.6 (0.0)	149.5 (11.5)	8.0 (0.1)
Low	Douglas-fir forest	Solid	6.8 (2.1)	1.2 (0.1)	0.3 (0.2)	0.7 (0.4)	0.3 (0.1)	3.3 (0.2)	0.3 (0.1)	295.2 (161.2)	6.5 (2.7)
		Particulate	7.7 (4.4)	1.0 (0.4)	0.7 (0.6)	1.1 (0.9)	0.2 (0.2)	3.5 (3.1)	0.2 (0.2)	ND (ND)	ND (ND)
		Aqueous	3.1 (2.8)	0.9 (0.3)	0.0 (0.0)	0.1 (0.1)	0.8 (0.5)	12.5 (9.5)	0.4 (0.1)	123.6 (44.8)	2.3 (1.3)
	Sagebrush shrubland	Solid	2.9 (0.3)	1.2 (0.1)	0.4 (0.1)	0.8 (0.2)	0.2 (0.0)	6.6 (0.1)	0.5 (0.1)	108.3 (20.1)	4.3 (0.8)
		Particulate	3.9 (1.2)	1.1 (0.6)	0.5 (0.3)	0.7 (0.4)	0.1 (0.1)	7.0 (4.1)	0.4 (0.2)	ND (ND)	ND (ND)
		Aqueous	1.1 (0.4)	0.9 (0.4)	0.0 (0.0)	0.0 (0.0)	0.3 (0.1)	17.4 (3.4)	0.9 (0.5)	72.4 (7.5)	3.2 (0.2)
Moderate	Douglas-fir forest	Solid	7.3 (3.0)	1.2 (0.1)	0.3 (0.1)	0.7 (0.2)	0.2 (0.1)	3.3 (0.2)	0.2 (0.1)	166.5 (68.5)	5.2 (0.6)
		Particulate	9.2 (5.2)	0.8 (0.3)	0.4 (0.2)	0.8 (0.4)	0.2 (0.1)	2.5 (1.0)	0.1 (0.1)	ND (ND)	ND (ND)
		Aqueous	3.7 (3.5)	1.3 (0.4)	0.0 (0.0)	0.2 (0.1)	0.6 (0.4)	18.9 (11.7)	0.6 (0.2)	87.1 (18.2)	1.8 (0.5)
	Sagebrush shrubland	Solid	2.8 (0.0)	1.2 (0.1)	0.4 (0.1)	0.8 (0.1)	0.2 (0.0)	6.5 (0.0)	0.4 (0.0)	27.8 (1.4)	0.9 (0.4)
		Particulate	2.7 (0.1)	0.8 (0.1)	0.2 (0.1)	ND (ND)	0.1 (0.0)	2.3 (1.4)	0.1 (0.1)	ND (ND)	ND (ND)
		Aqueous	4.6 (1.9)	13.7 (7.7)	0.0 (0.0)	ND (ND)	9.0 (0.9)	529.2 (49.5)	36.2 (4.0)	312.9 (129.4)	17.1 (3.9)
High	Douglas-fir forest	Solid	6.6 (1.5)	1.2 (0.0)	0.3 (0.1)	0.7 (0.2)	0.2 (0.1)	3.2 (0.1)	0.2 (0.0)	55.9 (16.4)	1.9 (0.9)
		Particulate	6.6 (1.4)	1.0 (0.1)	0.2 (0.1)	0.5 (0.1)	0.1 (0.0)	0.8 (0.4)	0.0 (0.0)	ND (ND)	ND (ND)
		Aqueous	3.8 (1.2)	2.7 (1.3)	0.0 (0.0)	0.3 (0.3)	6.2 (3.7)	167.1 (105.1)	12.7 (8.8)	132.7 (177.9)	4.3 (4.0)

Table S7. Molar stoichiometric ratios between Ca, Mg, Fe, Al, Na, K, S, C, and N to P. Mean and standard deviations are reported based on burn severity, vegetation type (Douglas-fir forest or sagebrush shrubland), and sample phase (solid samples, leachate particulate, or leachate aqueous).
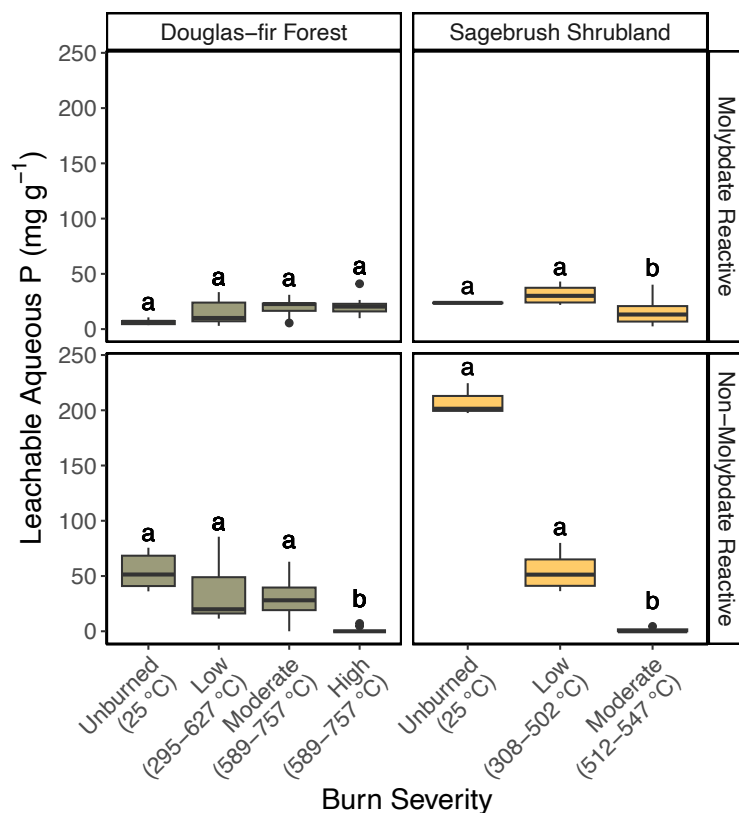
Figure S6. Leachable aqueous molybdate reactive P and non-molybdate reactive P (mg g^{-1}) for Douglas-fir forest (green) and sagebrush shrubland (yellow) based on burn severity classifications. Letters indicate significant differences between burn severities within each vegetation type (mixed effect model post hoc test). Non-molybdate reactive P was calculated as the difference between total P measured on ICP-OES and molybdate reactive P.
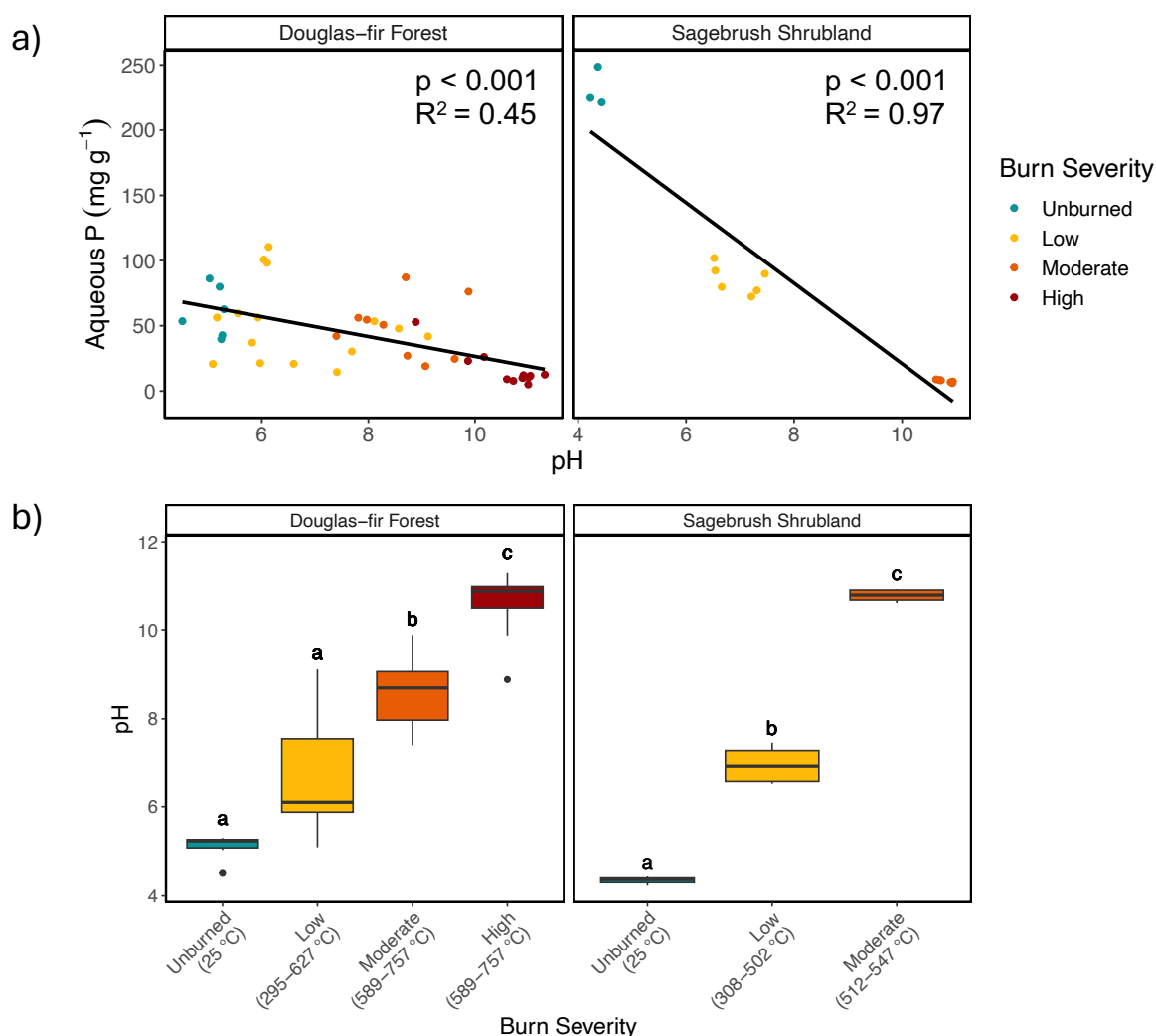
Figure S7. Relationship between a) pH and aqueous P for Douglas-fir forest and Sagebrush shrubland separately, and b) pH and burn severity, with letters representing significant ($\alpha = 0.05$) differences from post hoc test within the respective vegetation types.

References
Cade-Menun, B. J.: Improved peak identification in 31P-NMR spectra of environmental samples with a standardized method and peak library, Geoderma, 257–258, 102–114, https://doi.org/10.1016/j.geoderma.2014.12.016, 2015.

Doolette, A. L., Smernik, R. J., and Dougherty, W. J.: Spiking improved solution phosphorus-31 nuclear magnetic resonance identification of soil phosphorus compounds, Soil Sci. Soc. Am. J., 73, 919–927, https://doi.org/10.2136/sssaj2008.0192, 2009.

Grieger, S., Bailey, J., Barnes, M., Bladon, K. D., Forbes, B., Garayburu-Caruso, V. A., Graham, E. B., Goldman, A. E., Homolka, K., McKever, S. A., Myers-Pigg, A., Otenburg, O., Renteria, L., Roebuck, A., Scheibe, T. D., and Torgeson, J. M.: Organic Matter Concentration and Composition of Experimentally Burned Open Air and Muffle Furnace Vegetation Chars across Differing Burn Severity and Feedstock Types from Pacific Northwest, USA (V3), https://doi.org/10.15485/1894135., 2022.

Kruse, J., Abraham, M., Amelung, W., Baum, C., Bol, R., Kühn, O., Lewandowski, H., Niederberger, J., Oelmann, Y., Rüger, C., Santner, J., Siebers, M., Siebers, N., Spohn, M., Vestergren, J., Vogts, A., and Leinweber, P.: Innovative methods in soil phosphorus research: A review, J. Plant Nutr. Soil Sci. , 178, 43–88, https://doi.org/10.1002/jpln.201400327, 2015.

McDowell, R. W., Cade-Menun, B., and Stewart, I.: Organic phosphorus speciation and pedogenesis: analysis by solution ^{31}P nuclear magnetic resonance spectroscopy, Eur. J. Soil Sci., 58, 1348–1357, https://doi.org/10.1111/j.1365-2389.2007.00933.x, 2007.

Prietzel, J. and Klysubun, W.: Phosphorus K-edge XANES spectroscopy has probably often underestimated iron oxyhydroxide-bound P in soils, J. Synchrotron Radiat., 25, 1736–1744, https://doi.org/10.1107/S1600577518013334, 2018.

Ravel, B. and Newville, M.: ATHENA, ARTEMIS, HEPHAESTUS: data analysis for X-ray absorption spectroscopy using IFEFFIT, J. Synchrotron Radiat., 12, 537–541, https://doi.org/10.1107/S0909049505012719, 2005.

Recena, R., Cade-Menun, B. J., and Delgado, A.: Organic phosphorus forms in agricultural soils under Mediterranean climate, Soil Sci. Soc. Am. J., 82, 783–795, https://doi.org/10.2136/sssaj2017.10.0360, 2018.

Turner, B. L., Mahieu, N., and Condron, L. M.: Phosphorus-31 nuclear magnetic resonance spectral assignments of phosphorus compounds in soil NaOH–EDTA extracts, Soil Sci. Soc. Am. J., 67, 497–510, https://doi.org/10.2136/sssaj2003.4970, 2003.

Webb, S. M.: SIXpack: a graphical user interface for XAS analysis using IFEFFIT, Phys. Scr., 2005, 1011, https://doi.org/10.1238/Physica.Topical.115a01011, 2005.

Werner F, F.: LCF: Linear Combination Fitting. R package version 1.7.0, 2017.